FINAL REPORT

Multiscale Interaction of Turbulence, Temperature, and Soot Formation: Measurements for Critical Assessments of Chemical Kinetics and Mechanisms

Grant No: **DE-SC0019115**

Project Period: **8/1/2018 – 12/31/21**

Submitted on **September 13, 2022**

Submitted by

The Ohio State University
Office of Sponsored Programs
1960 Kenny Road
Columbus, OH 43210
DUNS 832127323

Jeffrey A. Sutton, Principal Investigator
Phone: 734-945-3501
Email: sutton.235@osu.edu

Submitted to **Department of Energy, Basic Energy Sciences, Gas-Phase Chemical Physics**

Multiscale Interaction of Turbulence, Temperature, and Soot Formation: Measurements for Critical Assessments of Chemical Kinetics and Mechanisms

Jeffrey A. Sutton, Ohio State University

Abstract

This program targeted an improved understanding of how turbulence affects soot formation chemistry (directly and indirectly) with a particular focus on detailing the multiscale coupling between flow turbulence, mixing, thermal transport, and soot formation kinetics in gas-phase reacting systems. In this project, simultaneous, quantitative multi-dimensional velocity, soot volume fraction, and gas-phase temperature measurements in turbulent non-premixed sooting flames were developed. These new diagnostics tools can be used to elucidate the relative effects of fluid kinematics, mixing, thermal processes, and turbulence/scalar time/length scales on soot formation chemistry and topology. Simultaneous multi-parameter measurements were acquired within a series of flames with different Reynolds numbers and spatial locations to investigate the inter-dependence of soot, temperature, and turbulence within the soot inception, growth, and oxidation region. Preliminary assessment of the results has been completed at the project end and detailed analysis is planned following the completed program.

1. Background

Soot occurs within many combustion-based energy conversion systems including ground transportation platforms such as diesel and direct-injection gasoline engines, power-generating and aviation gas turbines, and furnaces. Soot currently accounts for more than 25% of the total hazardous pollution in the atmosphere [1,2] and is a serious health concern due to its direct impact on the human respiratory and cardiovascular systems. Because of the detrimental effects on the environment and human life, soot emission from combustion platforms is regulated heavily. Meeting such stringent regulations is costly and time-consuming to engine designers and manufacturers when prototype testing and the application of empirically determined correlations is the primary methodology of "predicting" soot emissions. Ideally, a modeling capability would exist that is truly predictive; that is, a robust, flexible, physically based modeling approach that is capable of properly accounting for changes in fuel (chemical kinetics) and operating conditions. For the majority of energy-conversion systems, the operating environment is highly turbulent and thus it is imperative to understand (and ultimately predict) how soot formation, transport, and oxidation is modified when subjected to intense flow turbulence.

The underlying processes governing soot formation, growth, and destruction are thought to be well established. They include inception and nucleation involving polycyclic aromatic hydrocarbons (PAH) such as naphthalene; coagulation between existing soot particles; growth via surface condensation of PAH (naphthalene) or surface reactions via the hydrogen abstraction/C_2H_2 addition (HACA) mechanism; and oxidation with small molecules such as OH and O. These physio-chemical processes have been translated into detailed soot models which have been utilized for reasonably accurate computational predictions in various laminar flame configurations [e.g., 3-6]. However, when the same models are applied under turbulent flame conditions, significant disagreements between measurements and computational results occur (even if the gas-phase chemistry is predicted correctly). This leads to the conclusion that, at this time, no predictive capability exists for soot formation, transport and output under *highly turbulent* operating conditions.

The primary deficiency in soot prediction likely stems from an insufficient knowledge of how soot formation is modified under turbulent conditions with inaccurate descriptions of elementary kinetic processes contributing to a lesser degree. This lack of information is due, in part, to a limited amount of high-fidelity data that yields spatially and temporally resolved measurements that detail the rate-limiting physics and chemical processes in turbulent, sooting flames. For non-sooting flames, there are a large number of benchmark datasets used for understanding turbulence-chemistry interaction and model assessment, many of which have been generated through the International Workshop on Measurement and Computation of Turbulent Nonpremixed Flames (or "TNF workshop") [7]. The TNF workshop coordinates international collaboration between experimentalists and the modeling community systematically focusing on joint measurements and modeling/simulation within a progression of turbulent flames displaying increasing degrees of complexity in chemical kinetics, flow field dynamics, and overall turbulence-chemistry interaction. Non-intrusive laser-based techniques provide highly accurate measurements of flow field velocity, temperature, and species concentrations that are used isolate specific physio-chemical processes and assist in the development of physically based combustion models that are robust and predictive over a broad range of conditions.

In recent years the International Sooting Flame (ISF) workshop [8] has been developed based on the TNF workshop structure and identifies well-defined (sooting) target flames suitable for analyzing turbulence-soot interaction as well as model validation using various fuels. While there

has been substantial effort placed on producing reliable data, it is noted that many of the laser-based techniques that are applied effectively for quantitative flow field and scalar measurements under non-sooting conditions cannot be applied under sooting conditions. Of the laser diagnostics approaches that are feasible in sooting flames, they typically are much more difficult to apply and the quantification is subject to increasing levels of error as compared to their non-sooting counterparts. Michelsen [9] gives an overview of *in situ* diagnostic capabilities for probing soot formation, growth, and oxidation with a particular focus on particle diagnostics in laminar flames. However, she emphasizes that *needs* include methodologies for single-shot imaging in turbulent flames. In particular, there is a critical need for simultaneous multi-parameter measurements that can elucidate "cause and effect"; that is, measurements that can yield new information of the effects of turbulence on soot formation, its evolution, and fate.

2. Project Scope

This program targets an improved understanding of how turbulence affects soot formation chemistry (directly and indirectly) with a particular focus on detailing the multiscale coupling between flow turbulence, mixing, thermal transport, and soot formation kinetics in gas-phase reacting systems. There is ample evidence that soot formation and growth is strongly affected by turbulence. This is due to the fact that soot formation chemistry is characterized by slow time scales and thus surrounding fluid mechanic and mixing time scales not only influence the kinetic processes, but may dictate them. In this manner, the assessment of soot formation and the resulting chemical kinetic mechanisms for application under turbulent conditions must be benchmarked against measurements in turbulent reacting flows. This project targeted the development of simultaneous, quantitative multi-dimensional velocity, soot volume fraction, and gas-phase temperature imaging in turbulent non-premixed sooting flames to elucidate the relative effects of fluid kinematics, mixing, thermal processes, and turbulence/scalar time/length scales on soot formation chemistry and topology. The local gas-phase temperature field is critically important to further understand soot formation under turbulent conditions because of its direct linkage between turbulence (i.e., thermal and molecular mixing) and chemical kinetics (i.e., temperature-dependent reaction rates). In this program, a new implementation of filtered Rayleigh scattering (FRS) is applied for quantitative 2D temperature measurements in turbulent sooting non-premixed flames. The combined velocity (via PIV), soot volume fraction (via LII), and gas-phase temperature imaging provides a previously unavailable database concerning turbulence-temperature-soot interaction. From these measurements, novel multi-parameter statistics will be derived that detail the coupling and importance of various kinematic and thermal parameters. This analysis is necessary for understanding relevant formation pathways, transport mechanisms, and developing soot mechanisms to be applied under turbulent conditions.

3. Accomplishments

Development of Filtered Rayleigh Scattering Thermometry for Sooting Flames

While the implementation of laser-induced incandescence (LII) and particle imaging velocimetry (PIV) is difficult in sooting environments, the methods have been successfully applied [e.g., 10-13] and thus represent known measurement strategies under sooting conditions. The primary diagnostic challenge lies in developing and applying a robust and accurate temperature imaging methodology that can be applied in sooting turbulent non-premixed flames and simultaneously

with LII and PIV. Of the numerous laser-based thermometry approaches that exist, few are applicable in the presence of soot or PIV tracer particles due to the scattering/interference from the particles. In the current program, the targeted method for temperature measurements is filtered Rayleigh scattering (FRS). FRS is a variant of the traditional laser Rayleigh scattering (LRS) technique which uses the combination of a spectrally narrow laser and an atomic or molecular filter (cell filled with an absorbing species such as molecular iodine, I_2) placed in front of the detector [14]. This combination rejects interference that is spectrally identical to the incident laser light (i.e., scattered light from particles), while collecting gas-phase information. In this program we have developed particular fuel combinations for both non-sooting and sooting flames such that the measured FRS signal is a known function of temperature. This allows quantitative single-shot temperature measurements using only an FRS measurement.

Figure 1 shows a graphical representation of the FRS process. Scattering from soot and/or seeded PIV particles has the same spectral distribution (blue curve) as the incoming laser light with a very small Doppler shift that only is a function of velocity. If a spectrally narrow laser source is used, the particle scattering falls within the absorption band of the I_2 filter (dashed curve in Fig. 1) and will not make it to the camera. However, scattering from gas-phase molecules is spectrally-broadened and described by Rayleigh-Brillouin scattering (RBS; orange curve) which is a combination of Doppler broadening (random thermal motion of molecules) which gives rise to a Gaussian-shaped distribution and Brillouin sidebands, which are due to density disturbances (from the interaction of the laser and the gas) propagating as acoustic waves. Since the gas-phase RBS spectrum is broader than the I_2 absorption spectrum, a portion of the gas-phase scattering spectrum is transmitted to the camera (indicated by filled green regions in Fig. 1). If the particle scattering from the is suppressed by the I_2 filter, then the collected signal only represents gas-phase Rayleigh-Brillouin scattering and can be used to deduce temperature *without* interference from either the soot particles or the PIV tracer particles.

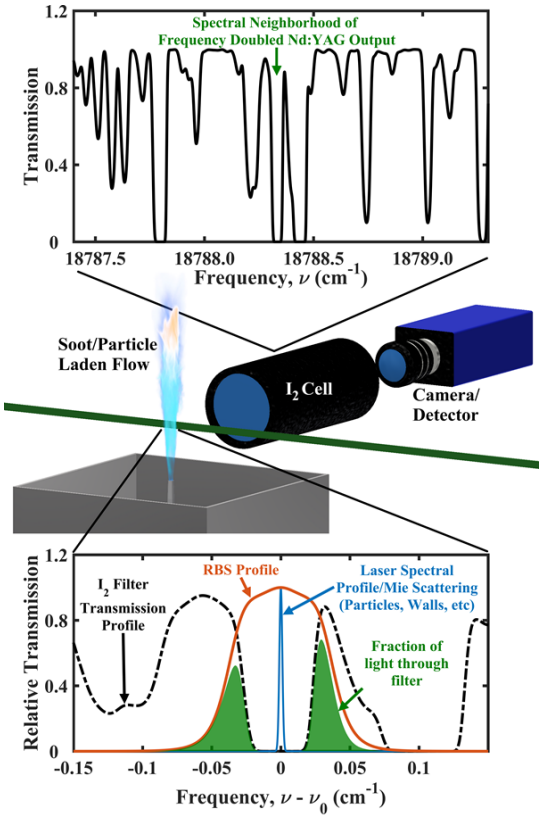

Fig. 1 – Filtered Rayleigh scattering (FRS) concept. The arrow within the I_2 spectrum indicates the particular I_2 absorption feature used for the proposed experiments.

The collected FRS signal can be written for a mixture as

$$S_{FRS} = AI_o n \sum X_i \sigma_i \psi_i(P,T,V,\nu,\theta) \qquad (1)$$

where A is a constant associated with the optics/imaging system, I_o is the incident laser intensity, n is the gas number density, X_i is the mole fraction of each species, σ_i is the differential Rayleigh scattering cross section for each species, and ψ_i is a FRS-specific variable, which is expressed as

$$\psi_i = \int_\nu \Re_i(P,T,V,\nu,\theta) T(\nu) \quad . \qquad (2)$$

In Eq. (1) it is assumed that the total FRS signal collected is a mole fraction-weighted sum of each species' individual FRS contribution. In Eq. (2) R_i is the Rayleigh-Brillouin scattering lineshape, T is the frequency-dependent transmission of the I_2 cell, and ν is the spectral frequency over which the RBS light and I_2 absorption bands are distributed.

In the current research program, a novel approach is taken, where "fuel tailoring" is used to develop a fuel mixture that allows quantitative single-shot temperature measurements in sooting turbulent non-premixed flames using only an FRS measurement. First, Eq. (1) is normalized by a reference measurement at known conditions, i.e., quiescent air at known pressure and temperature, T_{ref}:

$$\frac{S_{FRS}}{S_{FRS,air(T_{ref},V=0)}} = \frac{T_{ref}}{T} \times \boxed{\frac{\sum X_i \sigma_i \psi_i(T,V)}{\sigma_{air}\psi_{air}(T_{ref},V=0)}} \qquad (3)$$

In Eq. (3) it is assumed that all measurements are at a constant pressure, observation angle, laser frequency, and laser intensity; thus, their dependence is removed. In order to extract temperature from a single FRS measurement using Eq. (3), the dashed-boxed term would have to be unity. Due to the FRS signal dependence on the local mixture-averaged Rayleigh scattering cross section and the numerous species- and temperature-dependent RBS lineshapes, it is nearly impossible to satisfy this constraint. Alternatively, Eq. (3) is reformulated as

$$\frac{S_{FRS}}{S_{FRS,air(T_{ref},V=0)}} = \frac{T_{ref}}{T} \times \boxed{\frac{\sum X_i \sigma_i \psi_i(T,V)}{\sigma_{air}\psi_{air}(T,V)}} \times \frac{\sigma_{air}\psi_{air}(T,V)}{\sigma_{air}\psi_{air}(T_{ref},V=0)} \quad . \qquad (4)$$

In Eq. (4), the normalized FRS signal is represented by the product of three terms. The first term is the ratio of the known reference temperature to the local gas temperature. The second term is the ratio of $\sigma_i\psi_i$ of the local gas composition to the reference gas, air, at the *same temperature and velocity*. The third term is the ratio of the FRS signal transmission from air at the local temperature T and velocity V to that from air at the reference conditions (T_{ref}; $V = 0$); see Eq. (2). The goal of the current fuel tailoring strategy is to develop a fuel mixture such that the red boxed term in Eq. (4), also known as the figure of merit ($\mathcal{F}$), is unity with an acceptable error across the entire composition space of a turbulent sooting non-premixed flame. Assuming that the $\mathcal{F}$ is unity, the temperature is determined from an FRS measurement using

$$T = T_{ref} \times \frac{S_{ref}}{S_{FRS}} \times \frac{\psi_{air}(T,V)}{\psi_{air}(T_{ref},V=0)} \quad . \qquad (5)$$

where $S_{ref} = S_{FRS,air(Tref,V=0)}$ and the temperature dependence is embedded within the measured FRS signal and the temperature-dependent FRS response curve for air (second ratio in Eq. 5), which is calculated in a straightforward manner for air using the Tenti S6 model [15].

In this program, a fuel mixture has been designed such that $\mathcal{F} = 1 \pm \epsilon$, where $\epsilon \leq 0.03$ based on results from a series of laminar, opposed-flow non-premixed flame calculations which are part of a comprehensive FRS simulation tool developed within the PI's group. The total FRS simulation tool consists of calculations of (i) the I_2 absorption spectra using the model presented by Forkey [16], (ii) the RBS lineshapes of each species using the S6 Tenti model [15], and opposed flow simulations using the OPPDIF code [17] with the chemical kinetic mechanism from Narayanaswamy et al. [18] that is suitable for handling a range of complex hydrocarbons and soot precursors. Following a series of "trial and error" calculations, a fuel mixture of $0.12C_2H_2/0.45H_2/0.43Ar$ has been identified that both satisfies $\mathcal{F} \approx 1$ over the full operating space and the potential for sufficient soot production (discussed more in detail in Sec. 3.5). Figure 2

shows the results of applying Eq. (5) to the counterflow flame simulation results for the selected fuel mixture issuing into air. For the results, the simulated I_2 and laser properties are matched to standard experimental conditions; that is, the I_2 spectra were simulated at 341 K, a path length of 25 cm, and $P = 1$ Torr and the laser (and RBS profile) center frequency was 18788.334 cm^{-1}. Plotted in Fig. 2(a) are calculated temperatures as a function of mixture fraction, ξ (1 = pure fuel; 0 = pure air). The black, dashed line represents the 'actual' temperature from the counterflow flame simulation and the solid, red line represents the temperature which would be inferred from a single FRS measurement using Eq. (5) under these fueling conditions and the associated simulated FRS signals arising from the local composition from the OPPDIF simulation. Figure 2 (b) shows the value of $\mathcal{F}$ as a function of ξ, where the departure from $\mathcal{F} = 1$ represents the error in the methodology. The predicted FRS-based temperatures agree very well with the actual simulation temperatures, with values of $0.97 \leq \mathcal{F} \leq 1.03$ over the full range of operating conditions. Based on the results from the comprehensive FRS simulation tool as applied to laminar flame simulations, the proposed methodology of fuel tailoring shows great promise for enabling accurate temperature measurements in selected sooting non-premixed flames using a single FRS measurement.

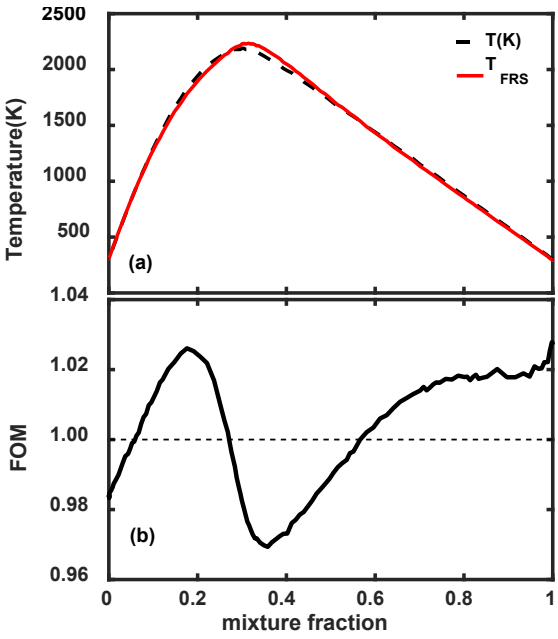

Fig. 2 – Simulated temperature accuracy using FRS thermometry. Results are from an OPPDIF simulation using a fuel of 12% C_2H_2, 45% H_2, and 43% Ar.

Experimental Assessment of the Accuracy of New FRS Thermometry Approach for Sooting Flames

The schematic of the experimental setup is shown in Fig. 3. The incident light source is an injection-seeded, frequency-doubled, Q-switched pulsed Nd:YAG laser operating at a pulse repetition rate of 10Hz. The laser output is tuned near 18788.335 cm^{-1}, which corresponds to the R56 (32,0) and P159(39,0)/P103(34,0)/P53(2,0) transitions of the B←X electronic system of I_2. A small portion (5%) of the incident laser is directed to a high-resolution wavemeter that monitors shot-to-shot laser spectral frequency output. For 1D measurements, the remaining laser output is focused with a 500-mm focal length spherical lens to a 100-μm (FWHM) spot size, while for the 2D imaging, the laser beam is focused through a 500-mm focal length cylindrical lens to generate a 100-μm-thick (FWHM), 8-mm-tall laser sheet. Three scientific-grade CCD cameras (PCO Sensicam) are used for signal collection. One camera is placed facing a uniform stream of air ("Air Jet") adjacent to the test section. This "energy correction" camera (EC CAM) collects LRS signals from the particle-free air in order to correct for shot-to-shot laser energy fluctuations and variations in laser sheet intensity distributions (for 2D imaging). The other two cameras are used for simultaneous FRS and LRS measurements within the flows of interest. A 248-mm long, 76-mm diameter iodine (I_2) cell is placed in front of the FRS camera. The I_2 cell is filled with an I_2 partial pressure of 126 Pa (0.96 Torr) and is wrapped by electrical resistance heat tape and heated to a temperature of 341 K. The LRS camera is placed adjacent to the FRS camera and focused to the same field-of-view. As discussed below, LRS measurements are recorded simultaneously with the

FRS measurements to serve as a temperature 'reference standard' of which to evaluate the FRS-based temperature measurements against.

A hierarchy of test configurations are used to evaluate the proposed FRS thermometry in different environments: 1) near-adiabatic premixed flat flames (soot free), and 2) laminar and turbulent sooting, non-premixed jet flames. A common burner platform used within the combustion community to assess diagnostic methods is the near-adiabatic flat flame "Hencken" burner [19]. This burner uses separate fuel and oxidizer streams that exit the burner surface in a series of small nozzle arrays. The reactants rapidly mix and ignite to produce a flat premixed flame that stabilizes above the burner surface, resulting is minimal heat loss to the surface and near-adiabatic flame conditions. The current Hencken burner has a 25.4×25.4 mm^2 exit and is surrounded by a coflowing inert gas (nitrogen) stream that both provides (i) a buffer against surrounding room air and (ii) a balance of momentum such that the flame is flat across the entire burner surface. Flow rates for each of the five gases are controlled by calibrated mass flow controllers. The air and fuel flow rates are varied to achieve the desired equivalence ratio (ϕ). For the current flames, the equivalence ratio is varied from 0.5 to 1.5 and the measurements are acquired at 18 mm above the burner surface. For each equivalence ratio, 500 measurements are taken and as described in Sec. 2, the measured in-flame FRS signals are normalized by reference measurements from a gas mixture of 86% N_2 and 14% O_2. Figure 3(b) shows a photograph of a rich (ϕ = 1.3) premixed flame stabilized above the surface of the near-adiabatic Hencken burner.

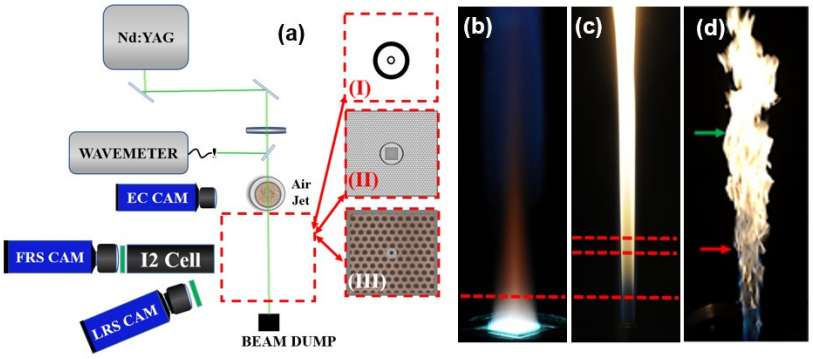

Fig. 3 – (a) Schematic of FRS and LRS optical setup using various configurations: (I) electrically heated gaseous jets, (II) near-adiabatic Hencken burner and (III) piloted non-premixed flames; (b) photograph of near-adiabatic premixed flame at ∅ = 1.3; the red dashed line indicates the measurement location; (c) photograph of laminar, sooting non-premixed jet flame; the red dashed lines indicate the measurement locations; (d) photograph of turbulent, sooting, non-premixed jet flame operating at Re = 11,000; arrows mark the center of the imaging field-of-view.

Finally, for the sooting non-premixed flames, the Sandia piloted burner [20] geometry is used. The fuel issues from a 7.4-mm-diameter circular tube surrounded by a 23-mm diameter pilot flame, although the pilot flame is not used for the current measurements. The two central streams are surrounded by a large 30 x 30 cm coflowing stream of air, operating at approximately 0.2 m/s and filtered to remove particulate. The Reynolds number, based on jet diameter, is 1,500 and 11,000 for the laminar and turbulent non-premixed flames, respectively. One thousand five hundred instantaneous LRS and FRS images are recorded at each measurement location for each operating condition. Figure 3(b) shows a photograph of the laminar non-premixed flame and Fig. 3(c) shows an instantaneous photograph of the turbulent non-premixed sooting flame using the proposed fuel mixture.

Near-Adiabatic Flames: The near-adiabatic, premixed Hencken burner presents a good in-flame environment to test the proposed FRS methodology (using the targeted fuel mixture) initially without the added complexity of soot interference. The accuracy of the proposed FRS-based approach is evaluated by comparing the derived temperatures using Eq. (5) to those from

LRS and FRS measurements in the same flames with accurate estimations of species concentrations. The methodology for determining the species concentrations for a given ϕ is outlined in [21]. Figure 4(a) shows a comparison between the derived temperatures as a function of equivalence ratio using the proposed FRS approach and the LRS- and FRS measurements using "known" compositions (denoted as '(w/ composition)' in the legend). First, it is noted that all measured temperatures are lower than the adiabatic temperature (T_{ad}; solid black curve) as expected because of heat loss to the burner. Second, the LRS-based and FRS-based temperature determined using the estimated species compositions agree with one another with to within 1%. Since the collected LRS and FRS signals have significant differences in temperature dependence and magnitude, the fact that they converge to the same temperature gives confidence in the estimated species composition and the derived temperatures. This provides an accurate temperature standard of which to assess the proposed FRS approach targeted for turbulent flames. The temperature values determined from the proposed FRS method deviate from the LRS- and FRS-based temperatures determined using species compositions by less than 5% fo r all equivalence ratios, with an average difference of 3% over the equivalence ratio range of 0.5 to 1.5.

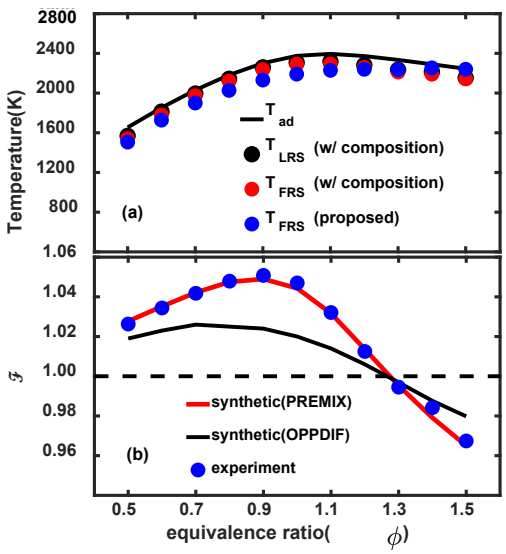

Fig. 4 – Comparison of derived temperatures using FRS and LRS with known species information ("truth") and the proposed FRS approach (Eq. 5). (b) Figure of merit as a function of mixture fraction for the proposed approach from measurements (symbols) and simulated flames (solid lines).

An important consideration for turbulent flame environments is the single-shot precision of the proposed FRS-based temperature measurement. The measurement precision or signal-to-noise ratio (SNR) can be determined from the steady, laminar flames as $\langle T_{FRS}\rangle/T_{rms}$, where $\langle T_{FRS}\rangle$ and T_{rms} are the mean and standard deviation, respectively, of the measurements from the proposed FRS thermometry approach. Over the equivalence ratios considered with temperatures ranging from 1500 K to 2250 K, the SNR is between 66 and 86. These results show that the proposed approach yields high SNR and measurement precision for single-shot measurements in turbulent flames.

Table 1: Statistics for FRS-Based Temperature Measurements in Near-Adiabatic Hencken Flames.

Equivalence ratio ϕ	$\langle T_{FRS}\rangle$[K]	T_{rms} [K]	SNR
0.5	1506	17.46	86.27
0.6	1727	22.06	78.28
0.7	1900	23.40	81.19
0.8	2027	27.04	74.96
0.9	2131	28.98	73.52
1.0	2191	33.28	65.83
1.1	2229	32.51	68.57
1.2	2240	30.81	72.71
1.3	2236	33.96	65.83
1.4	2254	31.42	71.74
1.5	2234	32.71	68.30

Non-Premixed Jet Flames: One-and two-dimensional temperature measurements are performed within laminar and turbulent non-premixed jet flames using the new FRS thermometry approach. For the laminar flame case (Re = 1500), measurements are taken at downstream positions of x/d = 3, 8, and 10, where d is the tube diameter. At measurement locations further

downstream than x/d = 10, scattering from soot particles is intense enough to saturate the LRS camera and thus measurements are not reported. Mean and RMS temperature profiles are determined from more than 1000 instantaneous FRS and LRS images. Figure 5 shows the mean temperature profiles determined from the LRS and FRS measurements. At the furthest upstream position (x/d = 3) the mean FRS and LRS-based temperatures show excellent agreement, with a small (~ 10 K) difference on centerline. Because this axial position corresponds to a non-sooting region, the LRS-based temperature is considered accurate and the agreement of the two approaches indicates accuracy of the proposed FRS approach for determining gas-phase temperatures. At the highest temperatures, the FRS-based measurements show much less noise (smoother curves) than the LRS measurements. At x/d = 8, the LRS-based temperature profile begins to exhibit artificial temperature reductions on both sides of the jet. These temperature reductions occur at slightly rich conditions and are a result of scattering from soot; that is soot scattering contributes to the local measured signal, which is artificially interpreted as artificially lowered temperatures. At the same locations, there are no apparent reductions in the measured FRS-based temperature. At x/d = 10, the soot concentration increases even further, leading to increased scattering contributions measured on the LRS channel. The extra signal leads to increases in the apparent reduction in the LRS-based temperatures in the sooty regions. In contrast, the FRS-derived temperature profile at x/d = 10 shows the expected profile shape for a laminar jet flame with no apparent effects from the local soot. The FRS-based profiles also show good agreement with LRS-based profiles outside the localized sooting regions. These results indicate that the proposed FRS thermometry approach does not appear to be affected by the presence of soot (at least for the current soot levels) and yields accurate gas-phase temperature measurements in both the non-sooting and sooting portions of the non-premixed flame environment.

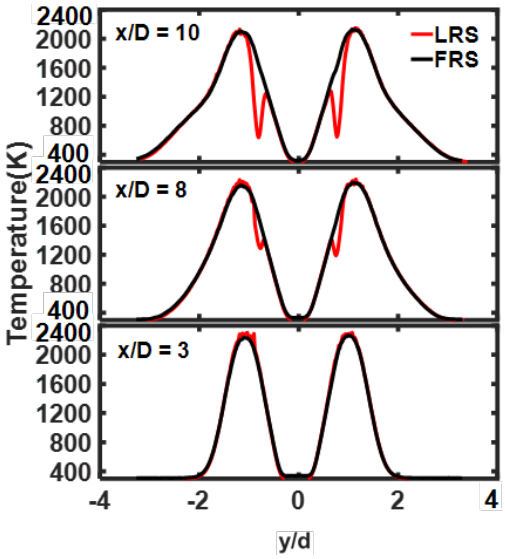

Fig. 5 – Mean temperature profiles in a laminar non-premixed laminar flame with at Re = 1500.

Subsequently, measurements in the Re = 11,000 turbulent non-premixed flame are performed at a downstream position of x/d = 5. Unlike the laminar non-premixed flame, the turbulent flame is unsteady and a comparison of LRS and FRS measurements only makes sense in the predominately non-sooting region due to the spatial intermittency of soot at position further downstream. Figure 6 shows a comparison of LRS/ FRS temperature profiles at x/d =5, which is considered a predominately non-sooting region based on visual inspection and the temperature measurements. The mean temperature profiles show excellent agreement with a small (< 20K) difference at centerline. Overall, the RMS profiles agree

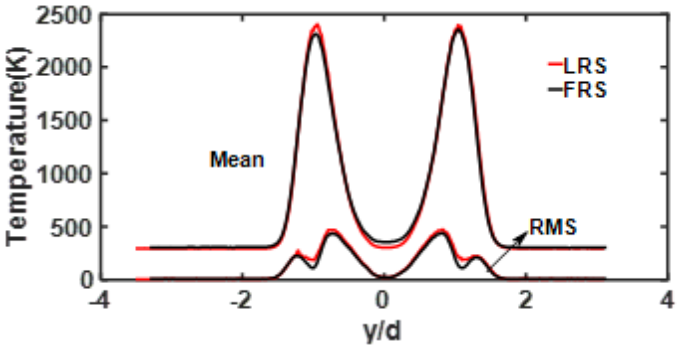

Fig. 6 – Comparisons of mean and RMS temperature profiles in a turbulent non-premixed turbulent flame at Re=11,000 using LRS- and FRS-based imaging. Measurements are performed at x/D = 5.

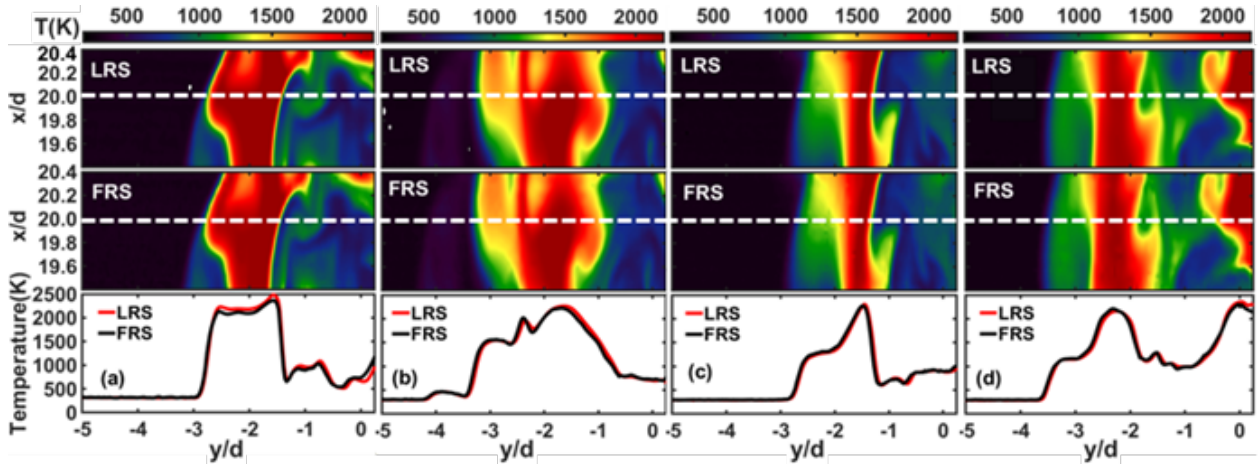

Fig. 7 – Example instantaneous 2D LRS- (top) and FRS-derived (middle) temperature images in the turbulent non-premixed flame. (Bottom)Transverse temperature profiles at x/d =20. Dashed line denotes the location of the extracted profiles.

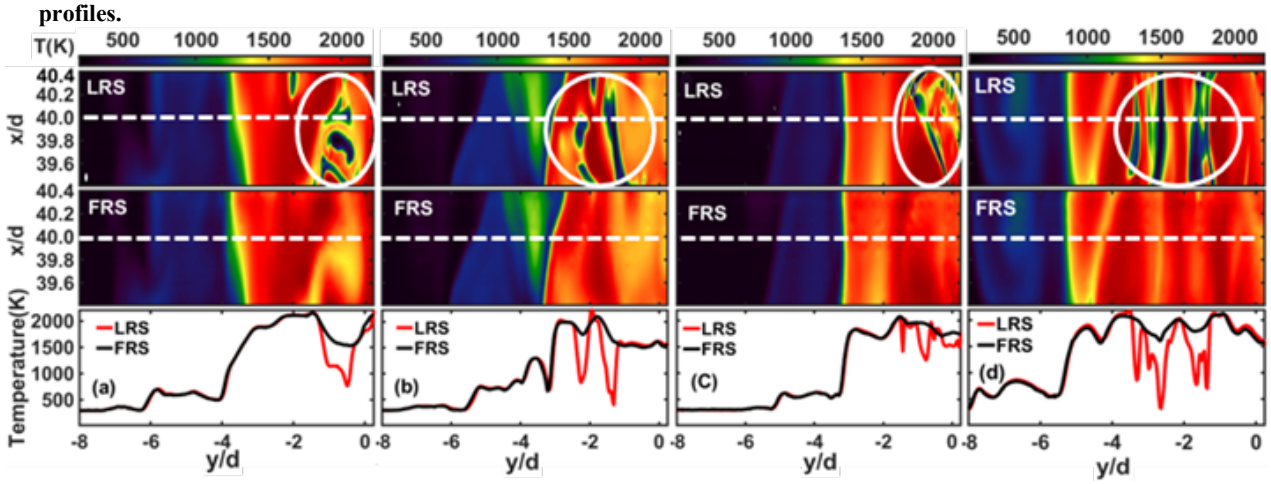

Fig. 8 – Example instantaneous 2D LRS- (top) and FRS-derived (middle) temperature images in the turbulent non-premixed flame. Circled areas highlight sooting regions. (Bottom)Transverse temperature profiles at x/d =40. Dashed line denotes the location of the extracted profiles.

well, with the LRS measurements showing slightly higher RMS values at y = ±1.2, which is near the peak temperature location. While this region is predominately non-sooting, occasional soot-laden samples are possible that lead to false reductions in the LRS-based temperature and increased variability (RMS fluctuations) compared to the FRS-based measurements, which are not affected by the presence of soot.

A series of instantaneous 2D LRS and FRS images are collected in the turbulent flame at x/d = 20 and x/d = 40. Figure 8 shows four examples of single-shot, 2D imaging at x/d = 20, along with sample extracted profiles at the location denoted by the white, dashed line in the images. At x/d = 20, both sooting and non-sooting examples exist. For the results shown in Fig. 7, only non-sooting examples were chosen to assess the accuracy of the proposed FRS measurements against the LRS measurements. The top images are temperature fields determined from LRS, while the middle row of images are the corresponding temperature fields determined from FRS. The LRS- and FRS-based temperature fields show excellent agreement and contain nearly identical topological features. The white dashed lines highlight the axial position at which one-dimensional transverse temperature profiles are extracted and the bottom sub-plots show a comparison of the temperature

profiles. The extracted temperature profiles indicate good agreement between LRS (red lines) and the proposed FRS thermometry approach (black lines).

Figure 8 shows four examples of single-shot, 2D temperature imaging at x/d = 40. For the results shown in Fig. 8, examples with notable soot levels are chosen. As in Fig. 7, the top images are the temperature fields determined from LRS and the middle row of images are from the proposed FRS thermometry approach. The circled regions in the LRS-based temperature fields qualitatively denote regions of high soot concentration, characterized by the abrupt change to localized regions of unreasonably low temperatures (from high scattering signals). As noted in Fig. 8 the LRS- and FRS-based images display nearly identical temperature fields, except in these sooting regions. The white dashed lines highlight the downstream location where the temperature profiles shown in the bottom row of Fig. 8 are determined. As expected from the temperature fields, the LRS and FRS temperature profiles show excellent agreement outside the presumed sooting regions. While the scattering from soot has visibly altered the LRS signal in these regions, the FRS-based temperature fields and extracted profiles show no visible effects. For example, in the regions denoted by the white circle, the FRS-based temperature fields display smooth gradients expected at this downstream location and many times display gradients with the opposite sign of the LRS measurements. This demonstrates that the proposed FRS approach appears to filter out the unwanted scattering from soot effectively.

Development of Particle Image Velocimetry (PIV) in Sooting Flames

Particle image velocimetry (PIV) is a critical part of the measurement program to understand how the various flow kinematic properties affect soot formation, growth, and transport. PIV in sooting flames is difficult due to the interference from the intense flame luminosity, which is primarily from the radiating soot. PIV image pairs typically are captured using an interline frame transfer camera, which allows the acquisition of two frames in quick succession. The first frame has an exposure time on the order of microseconds, while the second frame has an exposure time equal to the readout time of the first image which is on the order of 100 ms. Previous work [i.e., 22] has shown that the second PIV frames are affected significantly by luminosity and at times are

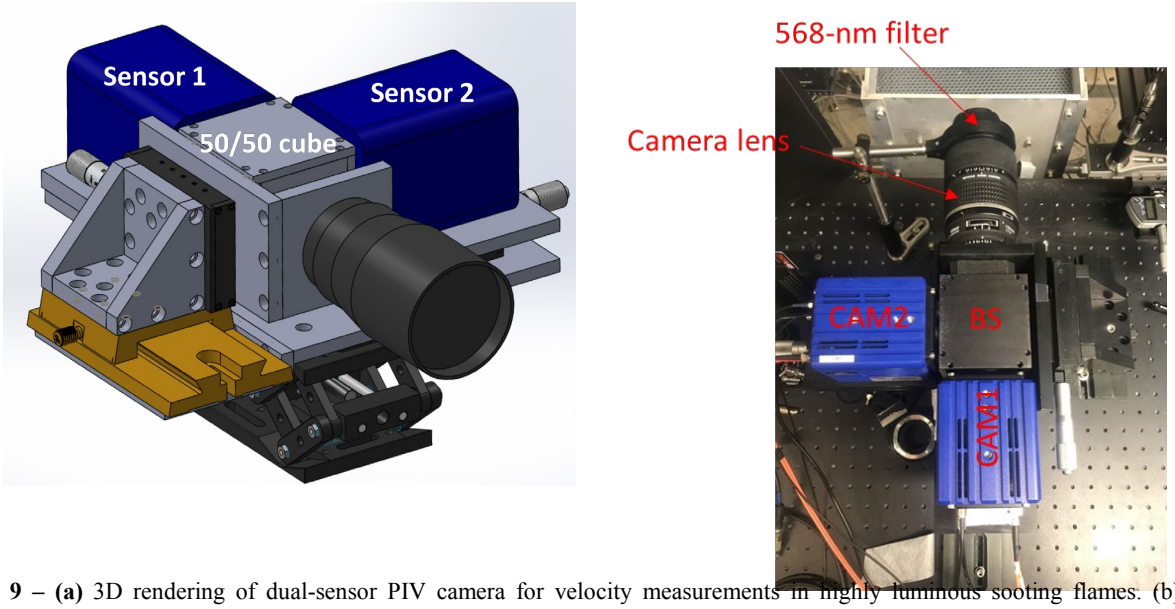

Fig. 9 – (a) 3D rendering of dual-sensor PIV camera for velocity measurements in highly luminous sooting flames. (b) Photograph of system.

unusable or lead to inaccurate velocity measurements at best. In the current program, we take an alternative approach for eliminating flame (soot) luminosity. We have designed and fabricated a dual-sensor PIV camera system that uses two ultra-high-resolution sCMOS cameras, each with a resolution of 2560 x 2160 pixels. A 3D rendering of the system is shown in Fig. 9a, while a photograph of the system is shown in Fig. 9b. The two camera sensors are coupled to a single lens through a 50/50 beamsplitter and sub-micron-level adjustment. In this manner, each camera sensor is responsible for one of the particle image pairs and thus, a short, microsecond-level shutter time is available for each PIV image and luminosity effects are minimized for each frame.

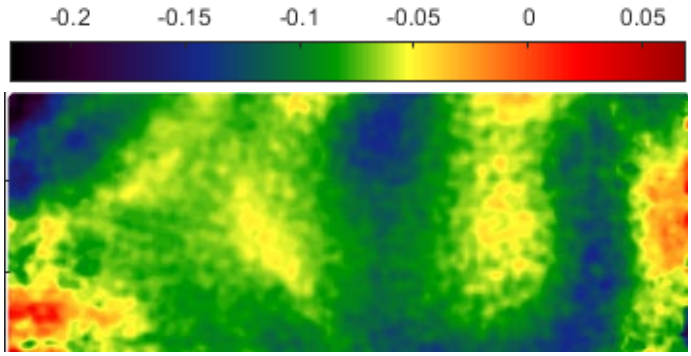

Fig. 10 – Pixel displacement due to misalignment of two camera sensors. This represents an error in the measurement

Validation of this approach is performed a turbulent jet (Re = 15,000). Both PIV measurements using the new dual-sensor (two integrated cameras) system and a traditional one-camera (two-frame) system is performed. For this assessment, we consider the one-camera system to serve as the "truth". Following calibration of the dual-sensor system, Fig. 10 shows that the new camera system has an uncertainty of < 0.2 pixels in particle displacement due to sensor mis-alignment. Figure 11 (top) shows an example result of a comparison between instantaneous velocity profiles extracted from both the dual-sensor and single-camera measurements in the turbulent jet, while Fig. 11 (bottom) shows the results of the mean velocity results. Both the instantaneous and velocity results show that the current dual-sensor PIV systems yields the same results as a traditional PIV system using one camera. Thus, our dual-sensor system – designed for highly luminous sooting environments – yields accurate results.

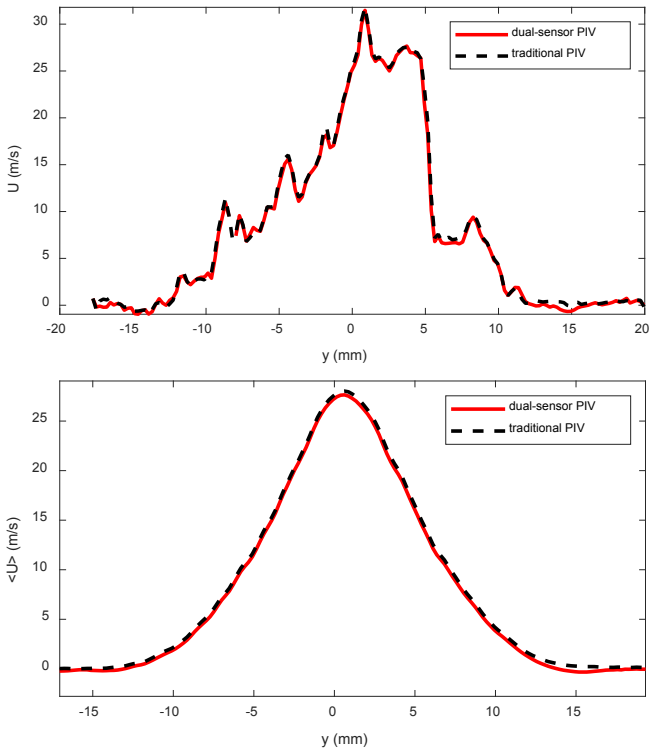

Fig. 11 – Comparison of (Top) instantaneous and (Bottom) average velocity results using the dual-sensor and traditional one-camera PIV.

Development of Quantitative Laser-Induced Incandescence (LII) in Sooting Flames

We developed quantitative soot volume fraction measurements using calibrated LII. Quantification is based on line-of-sight extinction measurements in a laminar, sooting, burner-stabilized flame. Figure 12 (top) shows a visible photograph of a premixed, $\phi = 2.3$, C_2H_4/air flame,

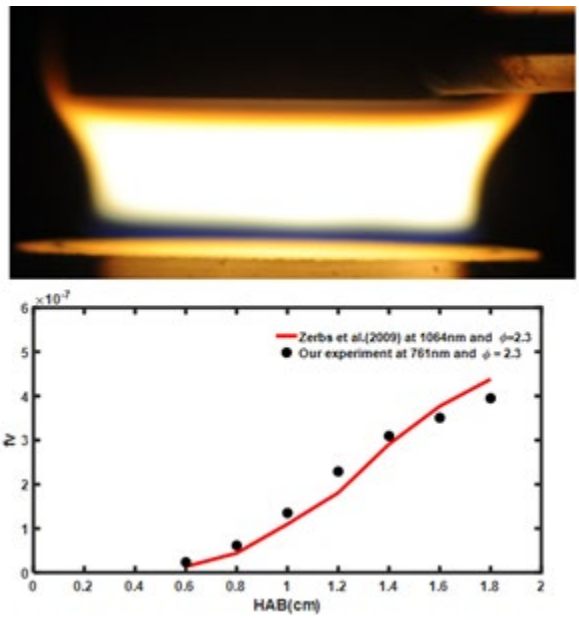

Fig. 12 – (Top) Photograph of premixed C2H4.air flame stabilized above the surface of a McKenna burner. (Bottom) Soot volume fraction measurements based on laser extinction as a function of height above the burner (HAB) surface.

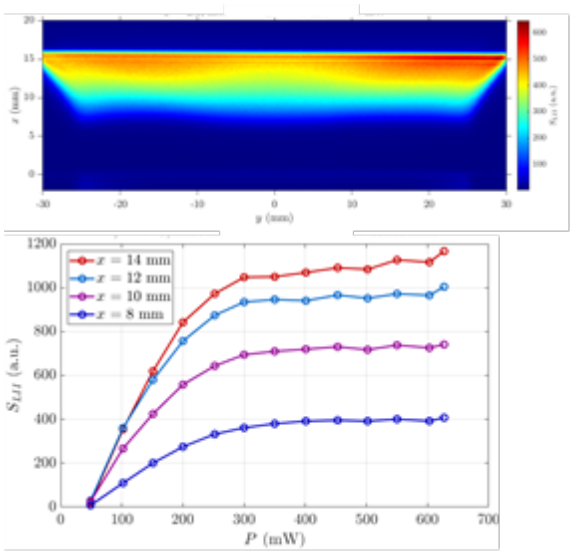

Fig. 13 –(Top) Average LII image from laminar, McKenna flame. (Bottom). Measurements of LII signal as a function of power (laser fluence).

stabilized above the surface of a water-cooled McKenna burner that serves as a standard calibration flame within the International Sooting Flame Workshop [7]. The bottom of Fig. 12 shows a comparison of the current extinction measurements acquired using a 761-nm diode laser with that of Zerbs et al. [23] at 1064 nm as a function of height above the burner (HAB) surface. The current laser wavelength was selected to minimize interference from water vapor in the flame. Excellent agreement is observed between the two data sets giving confidence in our calibration approach.

The next step is determining the appropriate laser fluence to use to ensure the measurements are in the so-called "plateau" regime, where the LII signal is independent of incident laser fluence. The measurements are taken with the camera gate set to 100 ns and the camera is outfitted with a 450-nm bandpass filter to collect blue-shifted incandescence. Figure 13 (top) shows an average LII signal in the McKenna flame and Fig. 13 (bottom) shows a series of measurements characterizing LII signal as a function of incident laser power for several positions above the burner surface. The incident laser fluence (F) is related to the laser power (P) as $F = P(tA)^{-1}$, where t is time and A is the laser sheet area. From the results, a laser power of approximately 300-400 mW (F = 0.7 J/cm^2) results in an LII signal that is independent of variations in laser fluence. Figure 14 reports measurements of LII signal as a function of soot volume fraction (fv) from all four heights. It is noted that there is a linear relationship between the soot volume fraction and the measured LII signal. This

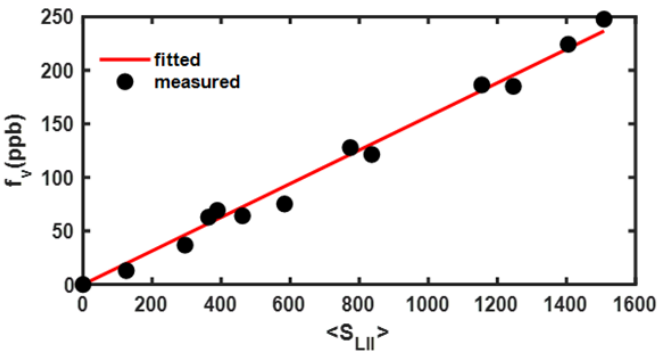

Fig. 14 – Relationship between measured LII signal and soot volume fraction in a laminar premixed flame at four different heights.

relationship can now be applied in turbulent flames for single-shot measurements.

Development of Simultaneous FRS, PIV, and LII Measurements

After development of each individual technique, the measurements were optimized together for multi-parameter measurements in a series of turbulent flames. The flames studied had Reynolds numbers of 10,000 and 20,000. Simultaneous FRS and PIV were performed in the non-sooting regions of the flame (x/d = 15) to parameterize the near-field mixing region. Simultaneous FRS, PIV, and LII were performed at 25-35 for the Re = 10,000 flame and at x/d = 45-55 for the Re = 20,000 flame to investigate the soot inception region. Further downstream, soot loadings were too high for FRS measurements and thus, simultaneous PIV and LII were performed to investigate the soot growth and oxidation regions. Figure 15 shows an example simultaneous FRS and LII image set at x/d = 30 in the Re = 10,000 flame. The images are displayed in acquired signal levels and have not been converted to temperature nor soot volume fraction. It is noted that FRS images (which can be converted to temperature) can be acquired without interference from moderate soot levels.

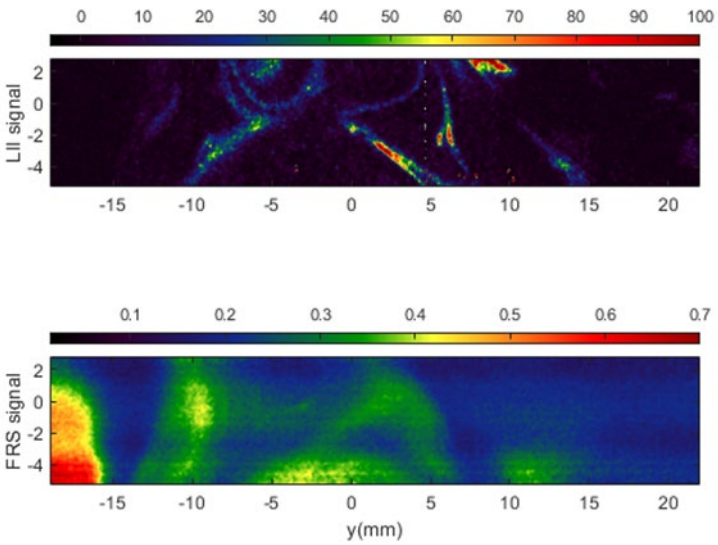

Fig. 15 – (Top) Instantaneous LII image which can be converted to soot volume fraction using the calibration shown in Fig. 14. (Bottom) Instantaneous FRS image which can be converted to temperature using the methodology outlined within this report.

Figure 16 shows a set of images acquired at x/d = 45 in the Re = 10,000 flame. The left-most images show the acquired particle images obtained in the first frame of both camera sensors within the dual-sensor system. The middle column displays the flame luminosity acquired on the second frame. The signal is more than 50,000 counts (out of 65,536 on a 16-bit sensor) and represent an insurmountable background interference with traditional PIV. The dual-sensor approach eliminates this interference. In the right-most column, the top image represents the LII signal acquired, while the bottom image represents the processed PIV field acquired within this heavily sooting region. Thus, we have successfully demonstrated simultaneous multi-parameter measurements in a heavily sooting turbulent flame.

4. Post-Project Pathway

At the time of this final report submission, all data has been acquired and image processed. However, there was insufficient time to perform post-processing and data analysis. Thus, research objectives have not been properly satisfied. The delay in acquiring the necessary data is primarily attributed to two major events that should be explained.

(1) This program was undertaken during the global pandemic due to Covid-19. Our laboratories were shut down in March 2020 and re-opened on a part-time basis in July 2020 and a full-time basis in January 2021. This lead to a six-month delay.

(2) While the laboratories were closed and subsequently re-started, many major pieces of equipment did not work properly when laboratories re-opened. For example, the primary laser and camera systems were down for two months.

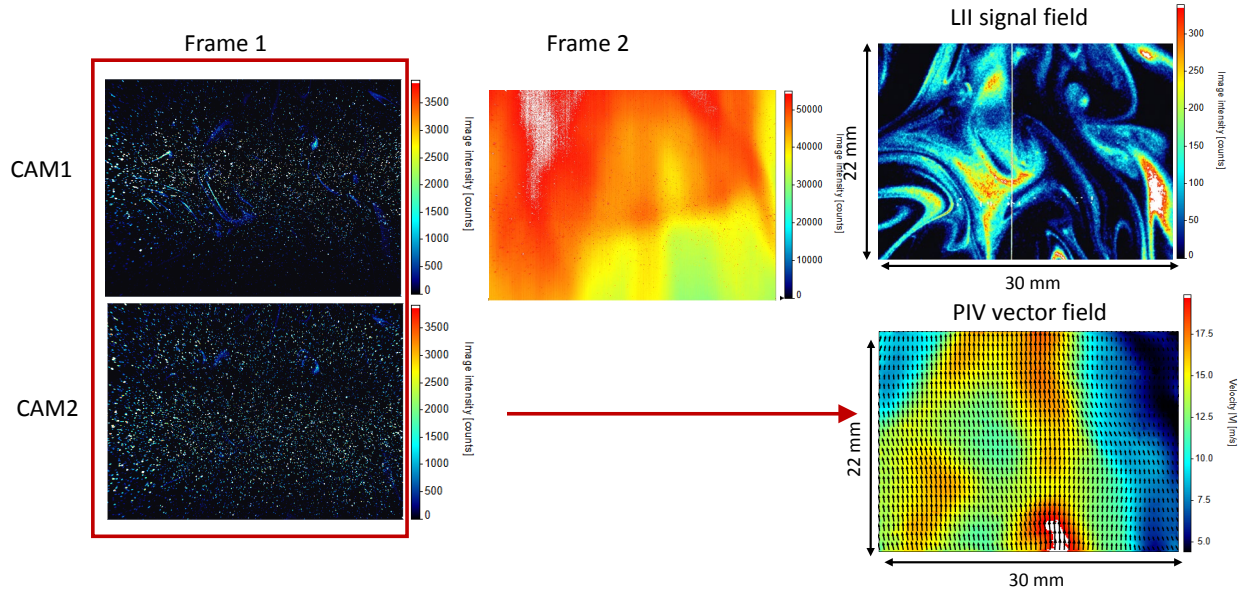

Fig. 16 – (Left) Sample particle images acquired in Re = 10,000 sooting flame. (Middle) Soot luminosity on second frame of interline-transfer cameras. This signal represents interference in traditional PIV. (Right) Top – sample soot field; Bottom – processed PIV field obtained in heavily sooting flame.

Overall, the unfortunate delays encountered within this program could not be made up within the remaining project time. The supported PhD student and part-time post-doctoral researcher worked tirelessly to make up a lot of the time. We do feel that the data could have been properly analyzed if we had not lost 8+ months on the project. However, there is a plan in place to continue to analyze the results and satisfy the bulk of the project goals after end-of-project. Discretionary funds are available to fund the graduate student who will ultimately use the data as part of his PhD dissertation (scheduled completion is May 2023). We will publish results with DoE BES acknowledgment.

After project's end, we will use the unique database acquired within the project to focus on **six** over-arching research goals – the primary goal of which is to understand how turbulence affects soot formation, growth, and oxidation: **(i)** analyze the structure of the fluctuating velocity, temperature, and soot volume fraction fields at various spatial regions within the flames including the soot inception, growth, and oxidation regions, **(ii)** directly compare soot formation in well-characterized laminar and turbulent flames, **(iii)** directly analyze the individual effects of Reynolds number and Damköhler number variations to understand how increasing turbulence levels and variations in turbulence-to-chemical time scales affects soot formation, **(iv)** characterize the primary mechanisms in which the turbulent flow and temperature fluctuations/gradients *modify and/or control* where and when soot is formed, **(v)** examine the effects of strain rate, thermal gradients, and dissipation rates on soot formation, growth, and topology, **(vi)** provide new multi-point, multi-parameter statistics to understand the correlation between velocity, temperature, and soot under turbulent flame conditions. These statistics also can be used to assess the capabilities of turbulent combustion models seeking to predict soot. This project has already yielded or will yield:

- Simultaneous spatially resolved velocity, temperature and soot volume fraction fields (complete)
- Simultaneous soot volume fraction fields overlaid on strain rate and dissipation rate fields (complete)
- Soot structural topology including intermittency, clustering, layer thickness, curvature, orientation, surface area and alignment with kinematic and scalar quantities (post project)
- Multi-point spatial correlations of velocity, temperature, and soot volume fraction (post project)
- Integral length scales of velocity, temperature, and soot volume fraction (post project)
- Temperature-velocity, temperature-soot volume fraction, and velocity-soot volume fraction correlations (post project)
- Multi-variate correlation analysis between soot volume fraction and other properties (i.e., velocity and temperature) and the corresponding multiple correlation coefficient (post project)
- Probability density functions of velocity, strain rate, temperature, and thermal gradients/dissipation rate conditioned on soot volume fraction (post project)
- Statistics of soot volume fraction conditioned on temperature and velocity and doubly conditioned statistics of soot volume fraction on temperature and velocity (post project)

Furthermore, the acquired data will specifically address the following questions which are fundamental to understanding soot formation chemistry and transport in turbulent sooting flames:

(i) What is the statistical relationship (including conditional moments) between soot volume fraction and the kinematic properties including velocity, vorticity, and strain rate? Can these statistical relationships yield new information on how the local turbulence *directly* affects soot formation?

(ii) What is the statistical relationship (including conditional moments) between soot volume fraction and temperature and thermal dissipation rate? Can these statistical relationships yield new information on how the local turbulence in*directly* affects soot formation?

(iii) How are instantaneous soot volume fraction values correlated with local velocity and temperature fluctuations? Which quantity, velocity or temperature, exhibits a higher correlation with the local soot volume fraction? Is this dependent on spatial position, local mixing rates, or the degree of soot loading itself?

(iv) How does the velocity-temperature-soot relationship change from laminar to turbulent flames? Is the relationship fundamentally different for laminar vs turbulent conditions? By studying a progression of flames from laminar to transitional to turbulent, can the rate-limiting kinematic and/or scalar processes that govern soot formation under highly turbulent conditions be isolated and identified?

(v) How does independently varying Damköhler number (fluid to chemical time scale ratio) and Reynolds number change velocity, temperature, and soot volume fraction statistics, including probability density functions, conditional statistics, multi-point and multi-parameter correlations, and integral length scales?

(vi) What roles do strain rate, vorticity, and thermal gradients play in the intermittent soot formation, topology, and its transport? Do soot structures preferentially align with the strain rate field? Do soot structures align along the thermal gradient or along isothermal contours? Is this a function of turbulence level or local time scales (i.e., Damköhler number)?

(vii) How does the local thermal (or scalar) dissipation rate affect local soot production; that is, how important is the rate of mixing in soot formation chemistry? Previous DNS studies observed an extreme sensitivity of the soot precursors to scalar dissipation rate, but the exact effect on the soot fields remained unclear.

(viii) Which set(s) of independent flowfield variables is soot production sensitive to? Which sets of independent variables are needed to describe local soot production? The coefficient of multiple correlation will be used to examine which subsets of variables (working in linear combination) have the largest influence on soot formation chemistry.

5. Opportunities for Training and Professional Development

This project supported the majority of the PhD work for Jinpeng Pu, who will finish his PhD degree in May 2023 and partially supported a post-doctoral researcher, Dr. Wesley Boyette. Mr. Pu received individual and customized training on advanced topics such as laser diagnostics, fluid mechanics, and combustion. Dr. Boyette was given the opportunity for mentoring on this project and closely supervised the work of Mr. Pu. Work from this program was submitted and presented at national conferences. Due to the Covid-19 pandemic, presentations were limited to virtual opportunities, but still provided opportunities for the research and results to be distributed. As part of this program, Dr. Boyette participated in the International Sooting Flames workshop.

6. References

1. Omidvarborna, H., Kumar, A., Kim, D-S., Characterization of Particulate Matter Emitted from Transit Buses Fueled with B20 in Idle Modes, *J. Env. Chem. Eng.*, 2014, 2(4), 2335-2342.
2. "Health Concerns Associated with Excessive Idling", NCTCOG.org, retrieved March 2017.
3. Blanquart G., Pitsch H., A joint volume-surface-hydrogen multi-variate model for soot formation. H. Bockhorn, A. D'Anna, A.F. Sarofim, H. Wang (Eds.), Combustion Generated Fine Carbonaceous Particles, KIT Scientific Publishing (2009), 437-463
4. Mueller M.E., Blanquart G., Pitsch H., Hybrid method of moments for modeling soot formation and growth, *Combust. Flame*, 2009, 156(6), 1143-55.
5. Mueller M.E., Blanquart G., Pitsch H., A joint volume-surface model of soot aggregation with the method of moments, *Proc. Combust. Inst.*, 2009, 1;32(1):785-92.
6. Blanquart G., Pitsch H., Analyzing the effects of temperature on soot formation with a joint volume-surface-hydrogen model, *Combust. Flame*, 156(8):1614-26.
7. International Workshop on Measurement and Computation of Turbulent Nonpremixed Flames, http://www.sandia.gov/TNF/abstract.html
8. International Sooting Flame (ISF) Workshop, http://www.adelaide.edu.au/cet/isfworkshop/

9. Michelsen, H.A., Probing Soot Formation, Chemical and Physical Evolution, and Oxidation: A Review of *in situ* Diagnostic Techniques and Needs, *Proc. Combust. Inst*., 2017, 36, 717-735.
10. Narayanaswamy, V., Clemens, N.T., *Combust. Flame*, 2013, 34, 1455-1463.
11. Köhler, M., Geigle, K.P., Meier, W., Crosland, B.M., Thomson, K.A., Smallwood, G.J., *Appl. Phys. B*, 2011, 104, 409-425.
12. Park, O., Burns, R.A., Buxton, O.R.H., Clemens, N.T., *Proc. Combust. Inst.,* 2017, 36, 899-907
13. Köhler, M., Boxx, I., Geigle, Meier, W., *Appl. Phys. B*, 2011, 103, 271.
14. Forkey, J.N., Finkelstein, N.D., Lempert, W.R., Miles, R.B., *AIAA J.* 1996, 34(3) 442.
15. Tenti, G., Boley, C.D., Desai, R.C., On the Kinetic Model Description of Rayleigh-Brillouin Scattering from Molecular Gases, *Can. J. Phys.*, 1974, 52(4), 285-290.
16. Forkey, J.N., Lempert, W.R., Miles, R.B., Corrected and Calibrated I2 Absorption Model and Frequency-Doubled Nd:YAG Laser Wavelengths, *Appl. Opt*., 1997, 36(27), 6729-6738.
17. Chemkin-PRO 15112, Reaction Design: San Diego, 2011.
18. Narayanaswamy, K., Pitsch, H., Pepiot, P., A chemical mechanism for low to high temperature oxidation of methylcyclohexane as a component of transportation fuel surrogates, *Combust. Flam*e, 2015, 162(4), 1119-1213.
19. Hancock, R. D., Bertagnolli, K. E., & Lucht, R. P. (1997). Nitrogen and hydrogen CARS temperature measurements in a hydrogen/air flame using a near-adiabatic flat-flame burner. *Combustion and Flame*, *109*(3), 323-331.
20. Masri, A.R., Dibble, R.W., Barlow, R.S., The Structure of Turbulent Nonpremixed Flames Revealed by Raman-Rayleigh-LIF Measurements, *Prog. Energy. Combust*. Sci., 1996, 22, 307-362.
21. Papageorge, M. J., Arndt, C., Fuest, F., Meier, W., & Sutton, J. A. (2014). High-speed mixture fraction and temperature imaging of pulsed, turbulent fuel jets auto-igniting in high-temperature, vitiated co-flows. *Experiments in fluids*, *55*(7), 1-20.
22. Köhler, M., Geigle, K.P., Meier, W., Crosland, B.M., Thomson, K.A., Smallwood, G.J., *Appl. Phys. B*, 2011, 104, 409-425.
23. J. Zerbs, K.P. Geigle, O. Lammel, J. Hader, R. Stirn, R. Hadef, W. Meier, *Appl. Phys. B* 96 (2009) 683-694.